Solute Concentrations in the Matrix of Zirconium Alloys Studied by Atom Probe Tomography

STP 1645, 2023 / available online at www.astm.org / doi: 10.1520/STP164520220026

Johan Eriksson,[1] David Mayweg,[1] Gustav Sundell,[1,2]
Hans-Olof Andrén[1], and Mattias Thuvander[1]

Solute Concentrations in the Matrix of Zirconium Alloys Studied by Atom Probe Tomography

Citation

J. Eriksson, D. Mayweg, G. Sundell, H.-O. Andrén, and M. Thuvander, "Solute Concentrations in the Matrix of Zirconium Alloys Studied by Atom Probe Tomography," in *Zirconium in the Nuclear Industry: 20th International Symposium*, ed. S. K. Yagnik and M. Preuss (West Conshohocken, PA: ASTM International, 2023), 149–172, http://doi.org/10.1520/STP164520220026[3]

ABSTRACT

This work indicates that the matrix content of the alloying elements iron, chromium, and nickel in as-produced commercial Zircaloy-2-type materials is lower than what has been indicated by many previous studies. Atom probe tomography in voltage pulse mode was used to study the matrix content of solutes in Zircaloy-2 of type LK3/L and a similar model alloy, called Alloy 2, of the same heat treatment. Both alloys were analyzed in the as-produced state and after reactor exposure. In the as-produced materials, the concentrations of iron, chromium, and nickel were all below the detection limits of around 10 wt. ppm. After reactor exposure, these alloying elements were observed to reside in clusters at <a> loops, and the matrix content (including clusters) of iron had increased to about 1,200 wt. ppm in the fueled region of the rod and to about half that value in the plenum region. The chromium content in the fueled region was approximately 100 wt. ppm, and the nickel content was approximately 200 wt. ppm. In the plenum region, the content of these elements was lower. However, due to an

Manuscript received February 18, 2022; accepted for publication May 9, 2022.
[1]Dept. of Physics, Chalmers University of Technology, SE-412 96 Gothenburg, Sweden
J. E. https://orcid.org/0000-0002-5794-7014, D. M. https://orcid.org/0000-0001-8013-1788,
G. S. https://orcid.org/0000-0002-6067-0175, H.-O. A. https://orcid.org/0000-0002-3583-5046,
M. T. https://orcid.org/0000-0002-6097-6895
[2]ESAB AB, SE-402 77 Gothenburg, Sweden
[3]ASTM 20th International Symposium on *Zirconium in the Nuclear Industry* held on June 20–23, 2022 in Ottawa, ON, Canada.

uneven distribution of clusters, there was a wide scatter in the measured concentrations in the irradiated materials. Additionally, the matrix concentrations of solute elements in (nonirradiated) Zircaloy-2 were investigated for a series of samples subjected to α annealing at 770°C followed by cooling at different rates. From these measurements, the solubilities at 770°C were estimated to be around 65 wt. ppm for chromium, at least 37 wt. ppm for iron, and below 9 wt. ppm for nickel. Slow cooling resulted in virtually no iron, chromium, or nickel in the matrix. The concentration of aluminum in the matrix was observed to be between 10 and 20 wt. ppm for all α-annealed samples and for the as-produced materials of commercial heat treatment.

Keywords

zirconium alloys, Zircaloy-2, nuclear fuel cladding, microstructure, heat treatment, solubility, matrix composition, irradiation, radiation damage, atom probe tomography

Introduction

Minor differences in chemical composition may have a large impact on the corrosion resistance and hydrogen pickup (HPU) of zirconium alloys during reactor operation.[1] Because the exact mechanisms of waterside corrosion and HPU of zirconium alloys are not fully known, it is not clear how the distribution of solutes in the matrix affects the in-reactor behavior. Observations of solute concentrations in the matrix before and after reactor exposure are therefore of interest.

In Zircaloy-2, small amounts of iron, chromium, and nickel are added to improve the corrosion resistance. Because these elements have low solubility in α-Zr, they form separate intermetallic phases, commonly known as second phase particles (SPPs), which are of two main types, $Zr(Fe,Cr)_2$ and $Zr_2(Fe,Ni)$, with varying iron/chromium and iron/nickel ratios in the precipitates.[2–5] It has been observed that some iron and nickel also reside at grain boundaries.[6,7] Tin and oxygen are added to improve the mechanical properties and are in solid solution in the matrix.[8] The tin content also affects the corrosion properties. Moreover, a number of trace elements are typically present in commercial Zircaloy-2 (e.g., carbon, nitrogen, aluminum, and silicon).[9]

At the alloying concentrations in Zircaloy-2, iron, chromium, and nickel are fully soluble in the β-Zr high-temperature phase. Upon β quenching, the material undergoes a phase transformation that leads to the formation of a Widmanstätten-type α structure, where the SPPs nucleate between the α lamellae.[10] Subsequent rolling and annealing steps result in coarsening and homogenization of the particle distribution, where the desired particle size is large enough to avoid excessive uniform corrosion but small enough to avoid localized nodular corrosion (in boiling water reactors [BWRs]).[8] The annealing parameters can be assumed to affect the content of alloying elements that remain dissolved in the metal matrix.

Attempts have been made to establish the exact concentrations of alloying elements in the zirconium matrix.[6,11–17] Due to the very low levels, it has proved

difficult to quantify the content using diffraction techniques because the lattice parameter is largely unaffected.[11] Hutchinson et al.[12] used thermoelectric power (TEP) measurements. TEP measurements are problematic for precise quantitative analysis because they require calibration. In Zircaloy-2, the method is applicable only for iron because no reliable calibration data exist for the other solutes. Results are also dependent on the cold-working steps,[18] making it difficult to compare different independent experiments. Yao et al.[13] attempted to measure the solute concentrations using wavelength-dispersive spectroscopy but concluded that the concentrations were lower than the detection limits of the method. Yilmazbayhan et al.[14] used synchrotron radiation microprobe X-ray fluorescence but were not able to distinguish between the smallest precipitates and the matrix. Zou et al.[15] used electron probe microanalysis and obtained iron concentrations in the Zircaloy-2 matrix of approximately 50–80 wt. ppm after annealing at temperatures between 500 and 800°C. Wadman and Andrén[16] and Kruger, Adamson, and Brenner[17] measured the solute concentrations in Zircaloy-2 and Zircaloy-4 of various heat treatments using 1D atom probe. These studies were problematic because the atom probe specimens easily fractured during the experiments, resulting in a limited statistical accuracy of the measurements. Wadman and Andrén[16] reported approximately 100–200 wt. ppm each of iron, chromium, and nickel in the matrix, and Kruger, Adamson, and Brenner[17] reported about 30 wt. ppm iron and 50 wt. ppm each of chromium and nickel. Hudson and Smith[6] used atom probe tomography (APT) to study the matrix of ZIRLO® and measured 30 at. ppm (about 18 wt. ppm) iron in the matrix.

In this study, the matrix chemistry of LK3/L Zircaloy-2 and that of Alloy 2 (a model alloy that is similar to the commercial alloy HiFi™ and has higher iron and chromium content than Zircaloy-2) were investigated using APT. This technique has the advantage of combining high mass resolution and very high spatial resolution, making it suitable for the determination of low levels of solutes in the metal matrix, easily avoiding any contribution from SPPs. Concentrations as low as a few tens of at. ppm, and sometimes even lower, can usually be detected.[19] In addition, Zircaloy-2 subjected to annealing at 770°C followed by cooling at different rates was analyzed with the aim of establishing the influence of various annealing parameters on the matrix composition. These materials are the same as those studied by Hutchinson et al.,[12] and the results were compared with the LK3/L Zircaloy-2 and Alloy 2. Finally, the effect of reactor operation on matrix chemistry in the latter two materials was studied.

Materials

LK3/L ZIRCALOY-2 AND ALLOY 2

The commercial (LK3/L-type) Zircaloy-2 and the Alloy 2 material were both supplied by Westinghouse. Both materials were in the as-produced state in the form of a fully recrystallized tube, having lot numbers 86788 (Zircaloy-2) and

86375 (Alloy 2). They had received heat treatments after the last β-quenching operation, corresponding to a heat treatment parameter of log $A = -14.2$ ($A = \Sigma_i\ t_i \exp(-Q/RT_i)$, where t_i is the time [s] and T_i the temperature [K] of the ith annealing and $Q = 63$ kcal/mol).[20]

In-reactor-exposed samples were taken from sibling fuel rods of the same lots as the as-produced materials. They had been exposed to an irradiation time of 2,082 days in the commercial BWR Oskarshamn 3. Zircaloy-2 samples were taken from elevations of 2,642–2,645 and 3,763–3,766 mm from the bottom of Rod 15-O3E9, and Alloy 2 samples were taken from elevations of 2,666–2,669 and 3,765–3,768 mm from the bottom of Rod 15-O3F9. The sample from the lower position of each rod was from the fueled region, and the sample from the upper position was from the plenum region, where the neutron flux was much lower, and they are referred to as high-fluence and low-fluence LK3/L Zircaloy-2 or Alloy 2, respectively. The calculated average burnup of the rods was 52 MWd/kgU. The composition of the LK3/L Zircaloy-2 and the Alloy 2 are shown in table 1.

α-ANNEALED ZIRCALOY-2

The Zircaloy-2 material was in the form of a 2-mm plate and was after β quenching annealed in the α phase at 770°C for either 5 or 300 min. From the annealing temperature, samples of both annealing times were cooled at three different rates: slow furnace cooling (FC) at an approximate rate of 0.03 K/s, air cooling (AC) at a rate of approximately 3 K/s, and water quenching (WQ) at a rate of approximately 300 K/s. After α annealing and cooling, the material consisted of α platelets approximately 10 μm wide, and SPPs were located at platelet boundaries. The maximum distance from a location in the matrix and the nearest SPP was thus approximately 5 μm. The heat treatments led to an average SPP size that was significantly larger than in commercial Zircaloy-2. Samples are designated 5WQ for 5 min of annealing time followed by WQ, and so forth. A more detailed description of the heat treatments is given in Hutchinson et al.[12] The composition of the alloy is presented in table 1, and figure 1 shows the SPP distribution in the 5WQ material. The content of iron in the matrix of the AC and FC materials was estimated by Hutchinson et al.[12] using TEP. Assuming that both WQ materials had a matrix iron content of

TABLE 1 Composition of the materials

Material	Fe (wt.%)	Cr (wt.%)	Ni (wt.%)	Sn (wt.%)	O (wt.%)	C (wt. ppm)	Si (wt. ppm)	N (wt. ppm)	Al (wt. ppm)
LK3/L Zry-2	0.18	0.13	0.061	1.49	0.12	143	91	40	< 30
Alloy 2	0.36	0.18	0.063	1.31	0.12	120	90	38	< 30
α-Annealed Zry-2	0.17	0.11	0.07	1.36	0.13	132	90	Not specified[a]	Not specified[b]

[a] < 80 wt. ppm according to the Zircaloy-2 standard.[21]
[b] < 75 wt. ppm according to the Zircaloy-2 standard.[21]

FIG. 1 Ion-induced secondary-electron image of the SPP distribution in the 5WQ material. SPPs give bright contrast in the image.

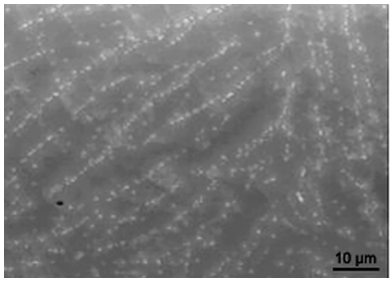

75 wt. ppm, the AC materials were estimated to contain 63–65 wt. ppm iron, and the FC materials were estimated to contain 47–51 wt. ppm iron.

Experimental Procedures

APT specimens were prepared using either electropolishing or the focused ion beam–scanning electron microscopy (FIB-SEM) lift-out technique.[22] For samples that were electropolished, thin rods ($0.3 \times 0.3 \times 15\ mm^3$) were cut. Electropolishing was then carried out in a two-step process in which the rod was first immersed in a layer of a solution of 10% perchloric acid, 20% glycerol, and 70% methanol floating on top of inert trichloroethylene. A positive potential of 18 V was applied to the rod until a neck had formed. The entire rod was then electropolished in 2% perchloric acid dissolved in 2-butoxyethanol at 15 V until a pair of sharp needles were formed. All specimens that were prepared using electropolishing were analyzed in laser pulse mode. For the LK3/L Zircaloy-2 and Alloy 2 specimens that were prepared using FIB-SEM, lift-outs were made approximately 40 µm from the outer surface of a cross section of the as-produced tubes and close to the metal/oxide interface of the in-reactor-exposed materials. The specimens prepared using FIB-SEM were analyzed in either laser or voltage pulse mode.

The analysis was performed using a local-electrode Imago LEAP 3000X HR atom probe, an instrument capable of both laser pulsing and voltage pulsing. Laser pulsing was carried out with monochromatic green light (wavelength 532 nm) at a pulse frequency of 200 kHz. Laser energies between 0.20 and 0.50 nJ were used. For voltage pulsing, pulse frequencies of 100 and 200 kHz and pulse fractions of 0.15 and 0.20 of the standing voltage were used. The temperature during most of the analyses was held at 70 K for both laser and voltage pulsing.

Zirconium-based materials are notoriously prone to fracture during atom probe analysis, especially when voltage pulsing is used.[16,17,23–25] Laser pulsing usually results in larger datasets than voltage pulsing, but the risk of fracture is large also

when laser pulsing is used. To get as long laser runs as possible, certain measures to prevent specimen failure were taken. During electropolishing a native oxide is formed on the needle surface. This oxide was removed from the tip by laser pulsing in the atom probe at relatively high temperatures (100–130 K) and a laser energy of 0.50 nJ.

The electric field strength at the end of the tip is a pivotal parameter because it determines the charge state of the ions that are evaporated from the tip. When analyzing Zircaloy-2 in the atom probe it is desirable to maintain a field strength in excess of 25 V/nm at the end of the tip. This will cause iron, chromium, and nickel ions to mainly evaporate as 2 + ions instead of 1+,[26] thus minimizing overlap with ZrC^{2+}, ZrO^{2+}, and Sn^{2+} in the mass spectrum. Voltage pulsing usually results in a higher field strength than laser pulsing and is therefore preferable when analyzing zirconium alloys. Voltage pulsing also appears to virtually get rid of CO^{+} ions that stem from adsorbed residual gas in the vacuum chamber and overlap Fe^{2+} in laser-pulsed mass spectra.[27] A comparison of a mass spectrum obtained using voltage pulsing and one obtained using laser pulsing is shown in **figure 2**. This comparison shows that the distribution of charge states for zirconium differs between the two pulsing modes, with higher fractions of Zr^{3+} and Zr^{4+} in voltage pulsing and higher fractions of Zr^{+} and Zr^{2+} in laser pulsing, a clear consequence of the higher field in voltage pulsing. It can also be seen that the background level is slightly higher in voltage mode.

The distribution of charge states for zirconium can be used to estimate the field strength during analysis.[26] From the Zr^{2+}/Zr^{3+} ratios of the obtained analyses, it was concluded that the field strength was approximately 26–27 V/nm during the analyses in laser pulse mode and 30–31 V/nm during the analyses in voltage pulse mode.

The gallium peak observed in the mass spectra is from gallium implanted during specimen preparation in the FIB. Furthermore, hydrogen, which commonly is observed in APT analyses of zirconium alloys,[25,28] is usually implanted during sample and specimen preparation, for example, in the FIB.[29,30] The hydrogen signal might also partly emanate from residual gas in the vacuum system of the APT instrument.[25,31] Oxygen, which is present as an alloying element, might additionally result from oxide formed on the specimen. For these reasons, gallium, hydrogen, and oxygen were excluded from the compositional analysis. Nitrogen, which is a common impurity in zirconium alloys, was not possible to separate from silicon in the mass spectra. Neither was it possible to separate silicon from CH_2. The stated values for silicon might, therefore, partly be due to nitrogen and CH_2.

The α-annealed Zircaloy-2 was analyzed in laser pulse mode, whereas the LK3/L Zircaloy-2 and Alloy 2 (both unirradiated and irradiated) were analyzed in voltage pulse mode. The use of laser pulsing for the α-annealed Zircaloy-2 might have resulted in a slight underestimation of the solute content due to the lower field during analysis but was chosen to collect large datasets. These measurements still

FIG. 2 Mass spectra obtained using voltage pulsing and laser pulsing. Each spectrum is from a specimen prepared using FIB-SEM of the α-annealed 300WQ material. The number of counts is 6.7 M in the voltage spectrum (*A*) and 12.2 M in the laser spectrum (*B*).

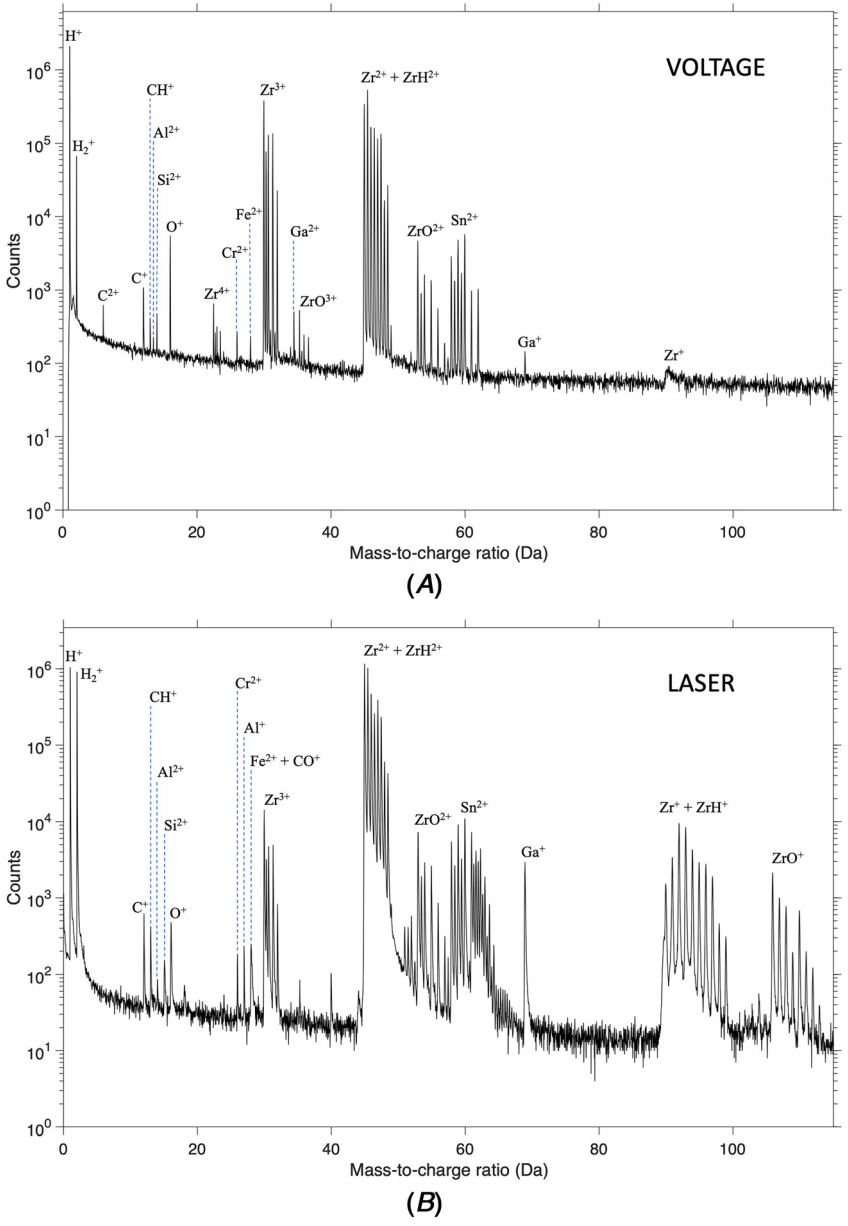

enable a comparison between samples of different heat treatments. Voltage pulsing was performed for one of the α-annealed samples to estimate the effect of using laser pulsing instead of voltage pulsing.

Data evaluation was performed using the software IVAS 3.6.14 from CAMECA. Doubly charged ions of iron, chromium, and nickel were used in determining the concentrations of these elements. For aluminum, singly or doubly charged ions were used depending on which species were observed, singly and sometimes also doubly charged in laser runs and doubly charged in voltage runs. Both singly and doubly charged carbon ions (including CH^+ at 13 Da) were used. The peak at 14 Da was ranged as silicon.

For peaks that were clearly above the background in the mass spectrum, background subtraction was done using the built-in (range-assisted) function in IVAS. The standard deviation was calculated using the counting statistics of the peak counts and the counts of the background. In runs in which there was no visible peak at the expected position (for chromium, iron, and nickel at 26, 28, and 29 Da, respectively), a range corresponding to a typical peak width for these positions (0.1 Da for voltage runs and equal to the width of the aluminum peak at 27 Da for laser runs) was placed symmetrically around the expected peak center. The detection limit for the respective element was calculated using the Currie definition,[32] as used in previous APT work.[33] According to the Currie definition, a detection limit in terms of number of counts equal to 2.71 plus 4.65 times the square root of the number of background counts can be used; a peak of this height would be detected 95% of the time. It should be noted that this detection limit is rather sensitive to the choice of range width.

The ion counts of all successful runs for each unirradiated material and condition were added. Quantification was then made using these accumulated counts. For the α-annealed Zircaloy-2, quantification was also done for the individual runs to study the variation between specimens. The same type of evaluation of the individual runs was done for the irradiated materials because the solute concentrations obviously vary depending on location, probably due to differences in the distance from SPPs that dissolve during irradiation.[28,34–37]

Results and Discussion

AS-PRODUCED LK3/L ZIRCALOY-2 AND ALLOY 2

The two most interesting parts of a typical APT mass spectrum, the ranges 5–15 and 22–34 Da, from the as-produced LK3/L Zircaloy-2 analyzed in voltage pulse mode are presented in **figure 3**. From this spectrum, which is also representative of the as-produced Alloy 2, it can be seen that carbon, aluminum, and silicon (or possibly nitrogen) are present, whereas iron, chromium, and nickel are not. **Table 2** presents the measured concentrations or calculated detection limits of these elements in the as-produced LK3/L Zircaloy-2 and Alloy 2, together with the total number of background-corrected ranged ions in the analyses.

FIG. 3 Mass spectrum in the ranges 5–15 and 22–34 Da obtained from voltage pulsing of the as-produced LK3/L Zircaloy-2. The absence of peaks at 26, 28, and 29 Da indicates levels of Cr, Fe, and Ni below the detection limits. Note that the peaks of Zr^{3+} located at 30–32 Da are truncated.

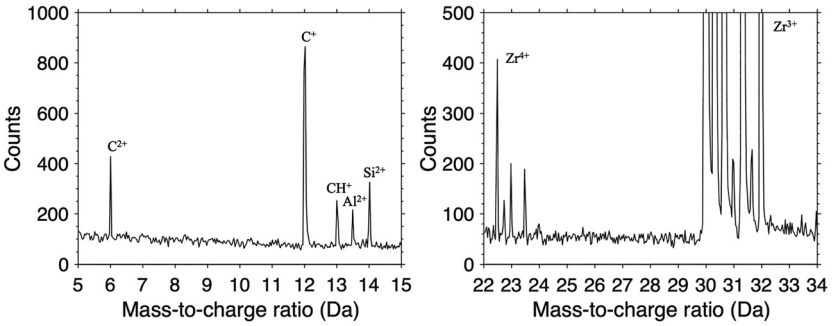

TABLE 2 Measured matrix solute concentrations in the as-produced LK3/L Zircaloy-2 and Alloy 2 in wt. ppm

Material	Fe	Cr	Ni	Al	Si	C	Total Number of Background-Corrected Ranged Ions (M)
LK3/L Zry-2	<12	<12	<16	18 ± 4	44 ± 5	113 ± 4	4.75
Alloy 2	<7	<7	<11	13 ± 2	31 ± 2	94 ± 2	15.6

Note: ± corresponds to two standard deviations of the counting statistics.

The measured carbon content corresponds to about 80% of the total carbon content of each material, and the silicon content corresponds to roughly one third to one half of the total silicon content. It should be kept in mind, however, that part of the silicon signal might be due to nitrogen or CH_2. The aluminum concentration was 18 and 13 wt. ppm in LK3/L Zircaloy-2 and Alloy 2, respectively. In table 2, the detection limits for nickel are higher than for iron and chromium. This is due to a slightly higher background at 29 compared with 28 and 26 Da and should not be interpreted as that there is more nickel than iron or chromium in the matrix of the materials. Due to the better statistics resulting from the larger number of ions in the Alloy 2 analysis, the detection limits for iron, chromium, and nickel were lower than in the LK3/L Zircaloy-2 analysis. Because there is more iron, chromium, and nickel in Alloy 2, and because the heat treatment of the materials is the same, there should not be a higher concentration of these elements in the matrix of LK3/L Zircaloy-2. It thus seems that the concentration of each of the elements iron, chromium, and nickel is below 10 wt. ppm in Zircaloy-2-type materials of this commonly used heat treatment.

α-ANNEALED ZIRCALOY-2

An APT mass spectrum, obtained using voltage pulsing, in the ranges 5–15 and 22–34 Da from the water-quenched 300WQ material is presented in figure 4, together with a corresponding spectrum obtained using laser pulsing. As expected, the charge states are higher for voltage pulsing; see, for example, the C^{2+}/C^{+} and Al^{2+}/Al^{+} ratios. The presence of peaks at 26 and 28 Da unambiguously shows the presence of chromium and iron, respectively. The wider peak at 28 Da in laser pulsing is probably a result of more adsorbed CO. There is no clear peak at 29 Da, indicating that the concentration of nickel is very low. The distribution of iron and chromium, as well as tin, was observed to be random, as shown in the atom map in figure 5. The small difference between the results of voltage and laser pulsing justifies the use of laser pulsing, which considerably improved the specimen yield (total number of ions collected per specimen).

The measured concentrations or calculated detection limits of iron, chromium, nickel, and aluminum in the matrix of the α-annealed Zircaloy-2 using all ions of the successful runs are presented in table 3, and the concentrations of iron,

FIG. 4 Mass spectra in the ranges 5–15 and 22–34 Da obtained from voltage and laser pulsing of the α-annealed 300WQ sample. Note that the peaks of Zr^{3+} located at 30–32 Da and the main peak of Zr^{4+} (voltage) located at 22.5 Da are truncated.

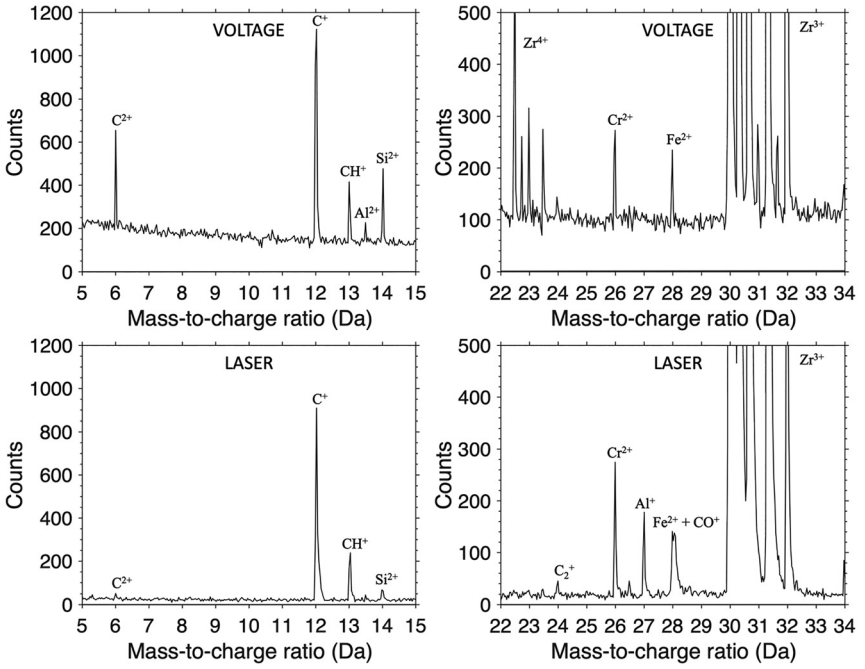

FIG. 5 Atom map showing the random distribution of Fe, Cr, and Sn in one of the 300WQ specimens.

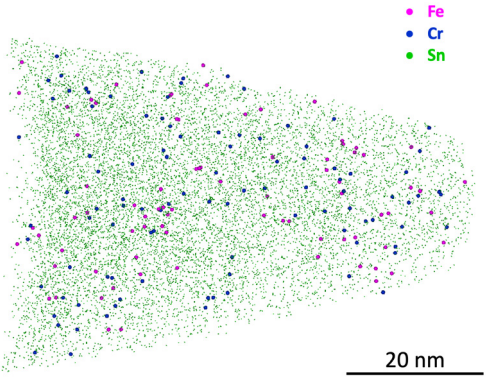

TABLE 3 Measured matrix solute concentrations in the α-annealed Zircaloy-2 in wt. ppm

Material	Fe	Cr	Ni	Al	Total Number of Background-Corrected Ranged Ions (M)
300WQ voltage	37 ± 4	65 ± 5	<9	10 ± 2	12.5
300WQ laser	38 ± 3	37 ± 3	<5	13 ± 1	12.9
5WQ laser	23 ± 2	54 ± 2	<2	15 ± 1	33.5
300FC laser	<8[a]	<8	<9	13 ± 4	2.2
5FC laser	<7[b]	<7[b]	<5[b]	11 ± 1	21.6

Note: ± corresponds to two standard deviations of the counting statistics.
[a]Estimated from the detection limit for Cr due to overlap with CO at 28 Da.
[b]Estimated from the run with highest concentration.

chromium, and aluminum of the individual runs are presented in figure 6 (in which nickel is not shown because it was below the detection limit in almost all analyses). A comparison of the results obtained using voltage pulsing and the results obtained using laser pulsing (for 300WQ) shows that there is only a small difference regarding the iron concentration, a slightly higher chromium concentration in voltage pulsing, and almost no difference regarding the aluminum concentration. Thus, our use of laser pulsing to obtain longer datasets should not have resulted in concentrations deviating much from concentrations obtained using voltage pulsing.

From the results in table 3 and figure 6, it can be seen that the approximate range for the concentration after WQ of iron and chromium, respectively, is 5–55 and 30–70 wt. ppm. After FC, the concentrations are very low—almost zero (i.e., below the detection limits). The concentration of aluminum is independent of

cooling time. Nickel was generally not observed in the analyses, with a few exceptions, indicating concentration gradients or enrichment at microstructural features.

Because the iron concentration in the AC material has been observed to be between that in the WQ and that in the FC materials,[12] a few runs each of the 300AC and 5AC materials were done to confirm this observation. The results of these runs indicate that the concentrations of both iron and chromium after AC are between the concentrations after WQ and FC. The results also confirm that aluminum is not affected by the cooling rate. Due to the rather poor statistics, AC is not included in **table 3** and **figure 6**.

To explain the results, differences in the diffusivity between the elements need to be considered. In α-Zr, the diffusion of iron and nickel is very fast. Chromium also diffuses fast, but much slower than iron and nickel. Using the data by Hood[38] for the tracer diffusion of iron, nickel, and chromium in pure zirconium, the diffusion length, $\sqrt{(Dt)}$, during 5 min at 770°C is approximately 170, 240, and 8 μm for iron, nickel, and chromium, respectively. The diffusion length needs to be several times longer than the maximum distance from a location in the matrix to an SPP to reach a constant concentration equal to the solubility limit. This distance is around 5 μm, so it is evident that before cooling starts the matrix has its equilibrium composition at this temperature for iron and nickel at both annealing times. For chromium the diffusion length during 5 min is approximately the same as the maximum distance to an SPP, and it is much larger (60 μm) during 300 min. Thus, the longer annealing time (300 min), but not the shorter time (5 min), should give the equilibrium chromium content at 770°C in the matrix. Instead, gradients in the chromium content between the center of the platelets and near SPPs can be expected in the material annealed for 5 min.

During cooling, the solubilities of iron, nickel, and chromium are expected to decrease significantly. In the binary Zr-Fe system, the solubility of iron (in equilibrium with Zr_3Fe) has been observed, with TEP, to decrease from 74 wt. ppm at 770°C to 3 wt. ppm at 570°C,[39] with similar results obtained using secondary-ion mass spectrometry (SIMS).[40] In the binary Zr-Ni system, the solubility of nickel has been observed, with SIMS, to be 9 wt. ppm at 800°C and 4 wt. ppm at 700°C.[41] Whether it is possible to retain a supersaturated composition of the matrix depends on the diffusion rate of solutes from the matrix to SPPs. Again using the data by Hood,[38] a rough estimate shows that after fast cooling at 300 K/s some 25% of the equilibrium iron content at 770°C will be retained in the center of the platelets, and composition gradients will be formed toward essentially no iron content close to SPPs. Even less nickel is expected to remain after quenching due to the faster nickel diffusion. By contrast, the diffusion of chromium is so much slower than that of iron and nickel (about three orders of magnitude smaller diffusion coefficient) that the chromium content should be decreased only close to SPPs; in platelet centers it should be essentially unaffected. In conclusion, we should expect some gradients in iron and nickel content in the 5WQ and 300WQ materials due to the fast cooling, and we should expect gradients in the chromium content in the 5WQ material.

FIG. 6 Concentrations of Fe (*A*), Cr (*B*), and Al (*C*) in the individual runs of 300WQ, 5WQ, 300FC, and 5FC.

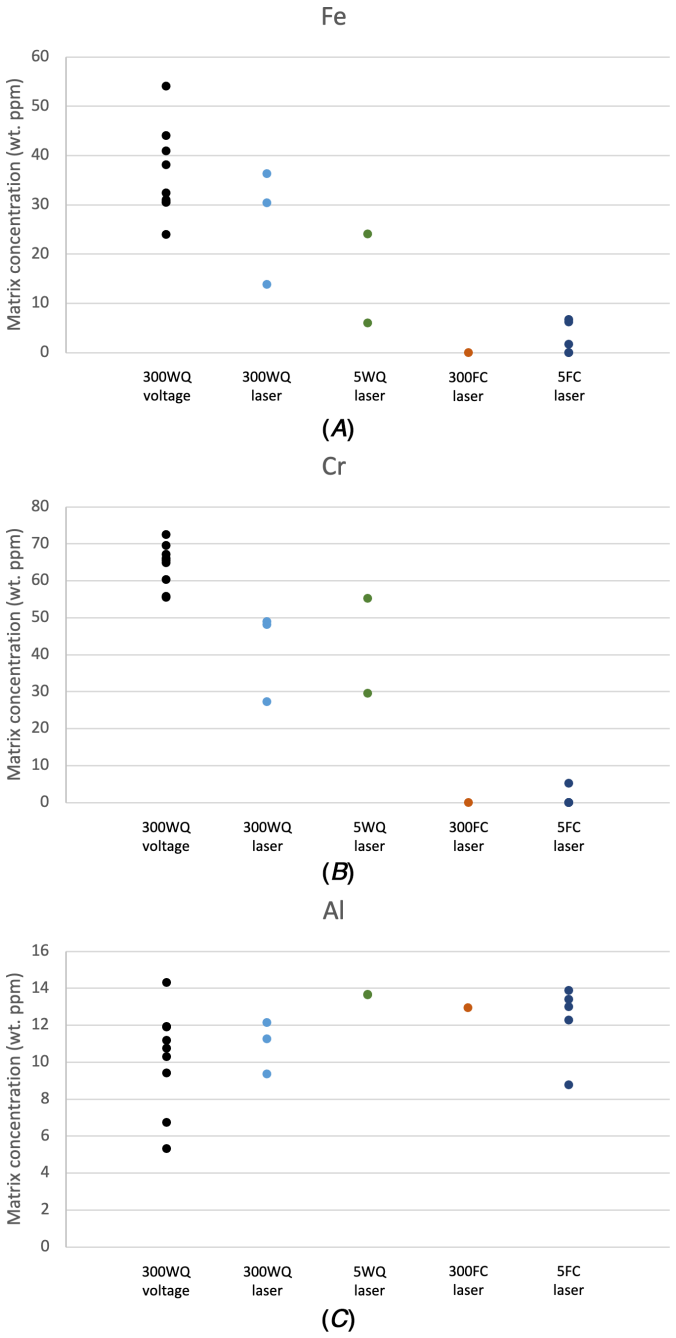

However, in the 300WQ material, the equilibrium content of chromium should be retained in most of the matrix, which thus can be estimated to 65 wt. ppm (using the voltage-pulsed data).

The supersaturation of iron and nickel should be effectively removed by fast diffusion during FC considering that diffusion lengths are a factor of 100 larger than for WQ. The supersaturation of chromium will also disappear after FC, in agreement with the experimental data.

The aluminum content in solid solution seems to be insensitive to cooling rate. This is expected due to the absence of an aluminum-rich phase in the material. The binary Zr-Al phase diagram also suggests some solubility.[42] The matrix content of aluminum in the α-annealed materials is about the same as in LK3/L Zircaloy-2 and Alloy 2 above.

The agreement between the TEP measurements and APT analysis of iron turned out to be rather poor. The concentration of iron determined from APT is significantly lower than what was previously estimated from TEP analyses.[12] One reason for this may be that in the interpretation of the TEP results only iron was assumed to contribute to the variation in TEP, whereas we now know that chromium varies more than iron (an approximate variation of 60 compared with 30 wt. ppm). Another problem is that the TEP measurements were calibrated against the WQ values for iron, which were both (5WQ and 300WQ) assumed to be 75 wt. ppm. According to our observations, they are below 40 wt. ppm.

It is thus possible to supersaturate the α-Zr matrix with small amounts of iron and particularly chromium at room temperature, provided that the cooling rate is very fast. However, the α-annealed Zircaloy-2 has from autoclave testing previously been observed to exhibit similar oxidation behavior with respect to heat treatment; a small difference between the two annealing times can be attributed to the coarsening of SPPs from around 165 to 225 nm.[12] Thus, it seems certain that the SPP size distribution is more important than the matrix content of iron, chromium, and nickel for the corrosion properties.

IN-REACTOR-EXPOSED LK3/L ZIRCALOY-2 AND ALLOY 2

An APT mass spectrum from the in-reactor-exposed high-fluence Alloy 2 analyzed in voltage pulse mode is presented in **figure 7**. The peaks of iron, chromium, and nickel are clearly visible, and the relatively high concentrations indicate that these elements have been dissolved from SPPs, in agreement with many previous studies.[28,34–37] No visual differences between the reconstructions of Zircaloy-2 and Alloy 2 specimens were observed. The atom map of a high-fluence Zircaloy-2 specimen shown in **figure 8** reveals clustering of iron, chromium, and nickel at what most likely are <a> loops, similar to previous observations.[28,34–37,43,44] Two main types of clusters were observed, disc-shaped Fe-Ni clusters and spheroidal Fe-Cr clusters, as observed previously.[43]

The measured solute concentrations in the matrix (including the clusters) after irradiation are shown in **table 4**. As expected, the concentrations are very much

FIG. 7 Mass spectrum in the ranges 5–15 and 22–34 Da obtained from voltage pulsing of the irradiated Alloy 2. Note that the peaks of Zr^{3+} located at 30–32 Da are truncated.

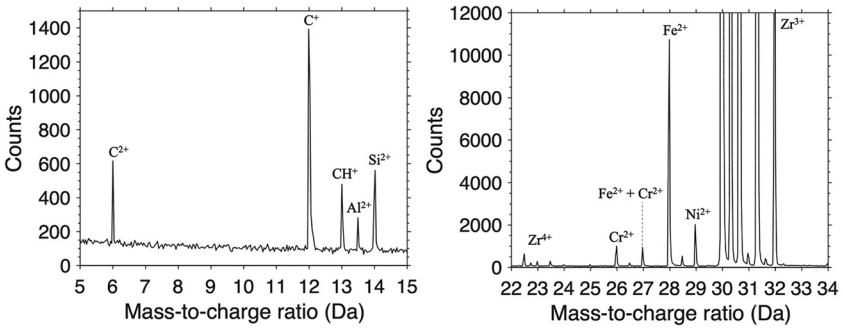

FIG. 8 Atom map showing the distribution of Fe, Cr, and Ni in an irradiated (high-fluence) LK3/L Zircaloy-2 specimen. Clusters of these elements are aligned in layers that are perpendicular to the <c> direction of the α-Zr matrix.

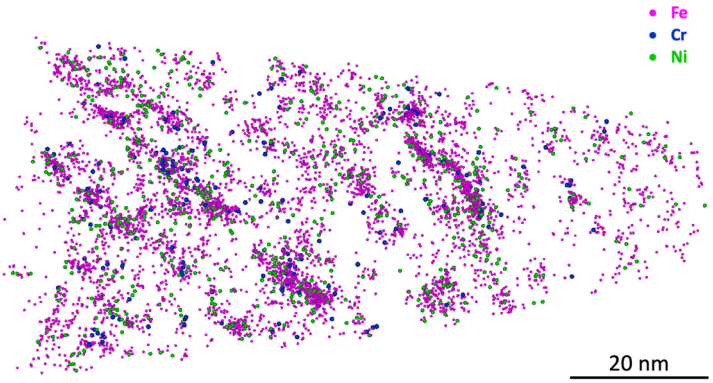

TABLE 4 Measured solute concentrations in the matrix (including clusters), average between specimens and range, in the in-reactor-exposed LK3/L Zircaloy-2 and Alloy 2 in wt. ppm

Material	Fe	Cr	Ni
High-fluence LK3/L Zry-2	1,210 (800–1,650)	120 (28–440)	160 (71–220)
High-fluence Alloy 2	1,150 (800–1,500)	81 (0–240)	240 (170–290)
Low-fluence LK3/L Zry-2	650 (530–880)	24 (0–68)	170 (120–340)
Low-fluence Alloy 2	650 (510–840)	15 (0–28)	110 (84–140)

higher than in as-produced materials due to the enrichment at irradiation-induced dislocation loops. The iron content is clearly higher than the chromium and nickel content and reaches about 1,200 wt. ppm iron in the fueled region of the rod and about half this value in the plenum region. The average chromium (~100 wt. ppm) and nickel (~200 wt. ppm) content in the fueled region is also much higher than in unirradiated materials and is higher than in the lower-fluence plenum region. However, due to inhomogeneities in the irradiated materials, there is scatter in the data, similar to previous observations.[28] There is no clear difference between LK3/L Zircaloy-2 and Alloy 2 despite the fact that the content of iron and chromium is higher in Alloy 2. This observation might be an indication that the loop number density, which (at the fluences of our samples) has been observed to increase with increasing fluence,[36,45] is decisive for the amounts of solutes that can be accommodated outside SPPs and grain and phase boundaries.

Previous APT work using laser pulsing has indicated a higher chromium than nickel content in the matrix (including clusters) after irradiation,[28,34,37] and previous APT work using voltage pulsing (on very few specimens) has indicated a higher nickel than chromium content.[43] The observation in this work of higher nickel than chromium content in several specimens using voltage pulsing thus suggests that voltage pulsing is needed to reliably detect nickel, although nickel is at least partly detected using laser pulsing.[28,34,37,46,47] From TEM studies it appears that chromium in irradiated Zircaloy-2 is mainly located close to SPPs, whereas nickel is more widespread in the matrix.[35,36] Observations of chromium being located in clusters mainly close to SPPs and grain or phase boundaries have been made using APT.[28,37] The difference in distribution between nickel and chromium is likely related to the difference in diffusivity.[38]

Conclusions

APT was used to study the matrix content of solutes in Zircaloy-2-type materials. LK3/L Zircaloy-2 was compared with a model material, Alloy 2, in the as-produced state and after operation in a BWR. Furthermore, α-annealed Zircaloy-2 was studied after different cooling rates. The following conclusions can be drawn:

- The matrix concentrations (excluding SPPs and grain boundaries) of iron, chromium, and nickel in the as-produced LK3/L Zircaloy-2, as well as Alloy 2, are below the detection limits, which are around 10 wt. ppm.
- In the matrix of water-quenched α-annealed Zircaloy-2, about 65 wt. ppm chromium was measured, suggesting that the solubility limit of chromium at 770°C is close to this value. The iron content was about 37 wt. ppm. Because iron diffusion is very fast, the solubility limit is somewhat higher than this value. The nickel content was below the detection limit.
- For the α-annealed Zircaloy-2, furnace cooling resulted in iron, chromium, and nickel matrix concentrations below the detection limits. Air cooling resulted in concentration values between those of water quenching and furnace cooling.

- After irradiation, iron, chromium, and nickel reside in clusters associated with <a> loops. In the in-reactor-exposed LK3/L Zircaloy-2 and Alloy 2, the matrix (including clusters) contains about 1,200 wt. ppm iron in the fueled region of the rod and about half this value in the plenum region. For chromium and nickel, the matrix in the fueled region contains approximately 100 and 200 wt. ppm, respectively. In the plenum region, the chromium and nickel content is lower. Due to the inhomogeneous cluster distribution, there was a wide scatter in the measured concentrations.
- The higher alloy content of iron and chromium in Alloy 2 did not result in higher matrix concentrations of these elements.

ACKNOWLEDGMENTS

This work was performed at the Chalmers Materials Analysis Laboratory. Material was made available via Westinghouse Electric Sweden AB and Bevis Hutchinson, Swerim AB. Westinghouse Electric Sweden AB, OKG AB, Vattenfall AB, EPRI, and SKC are gratefully acknowledged for their financial support. The MUZIC and MIDAS consortia are acknowledged for collaboration.

References

1. B. Cox, "Some Thoughts on the Mechanisms of In-Reactor Corrosion of Zirconium Alloys," *Journal of Nuclear Materials* 336 (2005): 331–368, https://doi.org/10.1016/j.jnucmat.2004.09.029
2. P. Chemelle, D. B. Knorr, J. B. van der Sande, and R. M. Pelloux, "Morphology and Composition of Second Phase Particles in Zircaloy-2," *Journal of Nuclear Materials* 113 (1983): 58–64, https://doi.org/10.1016/0022-3115(83)90166-6
3. M. Griffiths, R. W. Gilbert, and G. J. C. Carpenter, "Phase Instability, Decomposition and Redistribution of Intermetallic Precipitates in Zircaloy-2 and -4 during Neutron Irradiation," *Journal of Nuclear Materials* 150 (1987): 53–66, https://doi.org/10.1016/0022-3115(87)90093-6
4. X. Meng and D. O. Northwood, "Second Phase Particles in Zircaloy-2," *Journal of Nuclear Materials* 168 (1989): 125–136, https://doi.org/10.1016/0022-3115(89)90573-4
5. B. Cox and H. I. Sheikh, "Redistribution of the Alloying Elements during Zircaloy-2 Oxidation," *Journal of Nuclear Materials* 249 (1997): 17–32, https://doi.org/10.1016/S0022-3115(97)00191-8
6. D. Hudson and G. D. W. Smith, "Initial Observation of Grain Boundary Solute Segregation in a Zirconium Alloy (ZIRLO) by Three-Dimensional Atom Probe," *Scripta Materialia* 61 (2009): 411–414, https://doi.org/10.1016/j.scriptamat.2009.04.032
7. A. Baris, "Increased Hydrogen Uptake of Zirconium Based Claddings at High Burnup" (PhD thesis, University of Birmingham, 2019).
8. C. Lemaignan and A. T. Motta, "Zirconium Alloys in Nuclear Applications," in *Materials Science and Technology: A Comprehensive Treatment, Vol. 10B: Nuclear Materials, Part II*, ed. R. W. Cahn, P. Haasen, and E. J. Kramer (Weinheim, Germany: Wiley-VCH, 1994), 1–51.
9. L. S. Rubenstein, J. G. Goodwin, and F. L. Shubert, "Effect of Five Impurities on the High Temperature Water and Steam Corrosion Resistance of Zircaloy-2," *Corrosion* 18 (1962): 45t–54t, https://doi.org/10.5006/0010-9312-18.2.45

10. R. A. Holt, "The Beta to Alpha Phase Transformation in Zircaloy-4," *Journal of Nuclear Materials* 35 (1970): 322–334, https://doi.org/10.1016/0022-3115(70)90216-3
11. M. Ivermark, "Characterisation of the Matrix Chemistry in Zirconium Alloys" (PhD thesis, University of Manchester, 2009).
12. B. Hutchinson, B. Lehtinen, M. Limbäck, and M. Dahlbäck, "A Study of the Structure and Chemistry in Zircaloy-2 and the Resulting Oxide after High Temperature Corrosion," in *Zirconium in the Nuclear Industry: 15th International Symposium*, ed. B. Kammenzind and M. Limbäck (West Conshohocken, PA: ASTM International, 2009), 269–284, https://doi.org/10.1520/STP48141S
13. M. Y. Yao, Y. F. Shen, Q. Li, J. C. Peng, B. X. Zhou, and J. L. Zhang, "The Effect of Final Annealing after β-Quenching on the Corrosion Resistance of Zircaloy-4 in Lithiated Water with 0.04M LiOH," *Journal of Nuclear Materials* 435 (2013): 63–70, https://doi.org/10.1016/j.jnucmat.2012.12.029
14. A. Yilmazbayhan, O. Delaire, A. T. Motta, R. C. Birtcher, J. M. Maser, and B. Lai, "Determination of the Alloying Content in the Matrix of Zr Alloys Using Synchrotron Radiation Microprobe X-Ray Fluorescence," *Journal of Nuclear Materials* 321 (2003): 221–232, https://doi.org/10.1016/S0022-3115(03)00267-8
15. H. Zou, G. M. Hood, J. A. Roy, R. H. Packwood, and V. Weatherall, "Solute Distribution in Annealed Zircaloy-2 and Zr-2.5Nb," *Journal of Nuclear Materials* 208 (1994): 159–165, https://doi.org/10.1016/0022-3115(94)90207-0
16. B. Wadman and H.-O. Andrén, "Microanalysis of the Matrix and the Oxide-Metal Interface of Uniformly Corroded Zircaloy," in *Zirconium in the Nuclear Industry: Ninth International Symposium*, ed. C. M. Eucken and A. M. Garde (West Conshohocken, PA: ASTM International, 1991), 461–475, https://doi.org/10.1520/STP25522s
17. R. M. Kruger, R. B. Adamson, and S. S. Brenner, "Effects of Microchemistry and Precipitate Size on Nodular Corrosion Resistance of Zircaloy-2," *Journal of Nuclear Materials* 189 (1992): 193–200, https://doi.org/10.1016/0022-3115(92)90532-P
18. P. Merle, K. Loucif, L. Adami, and R. Borrelly, "Study of the Microstructural Evolution of α-Quenched or Cold-Rolled Zirconium Alloys during Isothermal Agings between 20 and 400°C," *Journal of Nuclear Materials* 208 (1994): 135–143, https://doi.org/10.1016/0022-3115(94)90205-4
19. P. H. Clifton, T. J. Gribb, S. S. A. Gerstl, R. U. Ulfig, and D. J. Larson, "Performance Advantages of a Modern, Ultra-High Mass Resolution Atom Probe," *Microscopy and Microanalysis* 14 (2008): 454–455, https://doi.org/10.1017/S1431927608087217
20. T. Andersson, T. Thorvaldsson, A. Wilson, and A. M. Wardle, "Influence of Thermal Processing and Microstructure on the Corrosion Behaviour of Zircaloy-4 Tubing," in *Improvements in Water Reactor Fuel Technology and Utilization* (Vienna, Austria: International Atomic Energy Agency, 1987), 435–449.
21. *Standard Specification for Zirconium and Zirconium Alloy Ingots for Nuclear Application*, ASTM B350/B350M-11 (West Conshohocken, PA: ASTM International, approved April 1, 2011), https://doi.org/10.1520/B0350_B0350M-11
22. K. Thompson, D. Lawrence, D. J. Larson, J. D. Olson, T. F. Kelly, and B. Gorman, "In Situ Site-Specific Specimen Preparation for Atom Probe Tomography," *Ultramicroscopy* 107 (2007): 131–139, https://doi.org/10.1016/j.ultramic.2006.06.008
23. B. V. Cockeram, K. J. Leonard, L. L. Snead, and M. K. Miller, "The Use of a Laser-Assisted Local Electrode Atom Probe and TEM to Examine the Microstructure of Zircaloy and Precipitate Structure Following Low Dose Neutron Irradiation at Nominally 358 °C," *Journal of Nuclear Materials* 433 (2013): 460–478, https://doi.org/10.1016/j.jnucmat.2012.10.006
24. A. J. Breen, I. Mouton, W. Lu, S. Wang, A. Szczepaniak, P. Kontis, L. T. Stephenson et al., "Atomic Scale Analysis of Grain Boundary Deuteride Growth Front in Zircaloy-4," *Scripta Materialia* 156 (2018): 42–46, https://doi.org/10.1016/j.scriptamat.2018.06.044

25. I. Mouton, A. J. Breen, S. Wang, Y. Chang, A. Szczepaniak, P. Kontis, L. T. Stephenson et al., "Quantification Challenges for Atom Probe Tomography of Hydrogen and Deuterium in Zircaloy-4," *Microscopy and Microanalysis* 25 (2019): 481–488, https://doi.org/10.1017/S143192761801615X
26. D. R. Kingham, "The Post-Ionization of Field Evaporated Ions: A Theoretical Explanation of Multiple Charge States," *Surface Science* 116 (1982): 273–301, https://doi.org/10.1016/0039-6028(82)90434-4
27. M. Thuvander and H.-O. Andrén, "Methods of Quantitative Matrix Analysis of Zircaloy-2," *Ultramicroscopy* 111 (2011): 711–714, https://doi.org/10.1016/j.ultramic.2010.12.008
28. J. Eriksson, G. Sundell, P. Tejland, H.-O. Andrén, and M. Thuvander, "Nanoscale Chemistry of Zircaloy-2 Exposed to Three and Nine Annual Cycles of Boiling Water Reactor Operation—An Atom Probe Tomography Study," *Journal of Nuclear Materials* 561 (2022): 153537, https://doi.org/10.1016/j.jnucmat.2022.153537
29. H. H. Shen, X. T. Zu, B. Chen, C. Q. Huang, and K. Sun, "Direct Observation of Hydrogenation and Dehydrogenation of a Zirconium Alloy," *Journal of Alloys and Compounds* 659 (2016): 23–30, https://doi.org/10.1016/j.jallcom.2015.11.031
30. S. M. Hanlon, S. Y. Persaud, F. Long, A. Korinek, and M. R. Daymond, "A Solution to FIB Induced Artefact Hydrides in Zr Alloys," *Journal of Nuclear Materials* 515 (2019): 122–134, https://doi.org/10.1016/j.jnucmat.2018.12.020
31. G. Sundell, M. Thuvander, and H.-O. Andrén, "Hydrogen Analysis in APT: Methods to Control Adsorption and Dissociation of H_2," *Ultramicroscopy* 132 (2013): 285–289, https://doi.org/10.1016/j.ultramic.2013.01.007
32. L. A. Currie, "Limits for Qualitative Detection and Quantitative Determination. Application to Radiochemistry," *Analytical Chemistry* 40 (1968): 586–593, https://doi.org/10.1021/ac60259a007
33. A. La Fontaine, S. Piazolo, P. Trimby, L. Yang, and J. M. Cairney, "Laser-Assisted Atom Probe Tomography of Deformed Minerals: A Zircon Case Study," *Microscopy and Microanalysis* 23 (2017): 404–413, https://doi.org/10.1017/S1431927616012745
34. G. Sundell, M. Thuvander, P. Tejland, M. Dahlbäck, L. Hallstadius, and H.-O. Andrén, "Redistribution of Alloying Elements in Zircaloy-2 after In-Reactor Exposure," *Journal of Nuclear Materials* 454 (2014): 178–185, https://doi.org/10.1016/j.jnucmat.2014.07.072
35. A. Harte, M. Topping, P. Frankel, D. Jädernäs, J. Romero, L. Hallstadius, E. C. Darby, and M. Preuss, "Nano-Scale Chemical Evolution in a Proton-and Neutron-Irradiated Zr Alloy," *Journal of Nuclear Materials* 487 (2017): 30–42, https://doi.org/10.1016/j.jnucmat.2017.01.049
36. A. Harte, D. Jädernäs, M. Topping, P. Frankel, C. P. Race, J. Romero, L. Hallstadius, E. C. Darby, and M. Preuss, "The Effect of Matrix Chemistry on Dislocation Evolution in an Irradiated Zr Alloy," *Acta Materialia* 130 (2017): 69–82, https://doi.org/10.1016/j.actamat.2017.03.024
37. T. Sawabe and T. Sonoda, "Evolution of Nanoscopic Iron Clusters in Irradiated Zirconium Alloys with Different Iron Contents," *Journal of Nuclear Science and Technology* 55 (2018): 1110–1118, https://doi.org/10.1080/00223131.2018.1479987
38. G. M. Hood, "Point Defect Diffusion in α-Zr," *Journal of Nuclear Materials* 159 (1988): 149–175, https://doi.org/10.1016/0022-3115(88)90091-8
39. R. Borrelly, P. Merle, and L. Adami, "Study of the Solubility of Iron in Zirconium by Thermoelectric Power Measurements," *Journal of Nuclear Materials* 170 (1990): 147–156, https://doi.org/10.1016/0022-3115(90)90406-D
40. H. Zou, G. M. Hood, J. A. Roy, R. J. Schultz, and J. A. Jackman, "The Solid Solubility of Fe in α-Zr: A Secondary Ion Mass Spectrometry Study," *Journal of Nuclear Materials* 210 (1994): 239–243, https://doi.org/10.1016/0022-3115(94)90177-5

41. H. Zou, G. M. Hood, H. Nakajima, J. A. Roy, and R. J. Schultz, "The Solid Solubility of Ni and Co in α-Zr: A Secondary Ion Mass Spectrometry Study," *Journal of Nuclear Materials* 223 (1995): 186–188, https://doi.org/10.1016/0022-3115(95)00023-2
42. J. Murray, A. Peruzzi, and J. P. Abriata, "The Al-Zr (Aluminum-Zirconium) System," *Journal of Phase Equilibria* 13 (1992): 277–291, https://doi.org/10.1007/BF02667556
43. J. Eriksson, G. Sundell, P. Tejland, H.-O. Andrén, and M. Thuvander, "An Atom Probe Tomography Study of the Chemistry of Radiation-Induced Dislocation Loops in Zircaloy-2 Exposed to Boiling Water Reactor Operation," *Journal of Nuclear Materials* 550 (2021): 152923, https://doi.org/10.1016/j.jnucmat.2021.152923
44. B. M. Jenkins, J. Haley, M. P. Moody, J. M. Hyde, and C. R. M. Grovenor, "APT and TEM Study of Behaviour of Alloying Elements in Neutron-Irradiated Zirconium-Based Alloys," *Scripta Materialia* 208 (2022): 114323, https://doi.org/10.1016/j.scriptamat.2021.114323
45. T. Ungár, P. Frankel, G. Ribárik, C. P. Race, and M. Preuss, "Size-Distribution of Irradiation-Induced Dislocation-Loops in Materials Used in the Nuclear Industry," *Journal of Nuclear Materials* 550 (2021): 152945, https://doi.org/10.1016/j.jnucmat.2021.152945
46. G. Sundell, M. Thuvander, and H.-O. Andrén, "Enrichment of Fe and Ni at Metal and Oxide Grain Boundaries in Corroded Zircaloy-2," *Corrosion Science* 65 (2012): 10–12, https://doi.org/10.1016/j.corsci.2012.08.061
47. T. Sawabe, T. Sonoda, and S. Kitajima, "Analysis Method of Matrix and Second Phase Particles in Zircaloy-2 by Atom Probe Tomography," *Progress in Nuclear Energy* 82 (2015): 159–164, https://doi.org/10.1016/j.pnucene.2014.07.012

Discussion

Questions from Brian Cockeram, Naval Nuclear Laboratory, Bettis Laboratory:

1. Can you comment on the size of the iron and chromium clusters in comparison to the <a> loops?
2. Can you give the number density of iron and chromium clusters in comparison to the <a>-loop number density?
3. Were there iron and chromium clusters observed that were not associated with <a> loops (i.e., was the number density of clusters of iron and chromium higher than that for the <a> loops)?

Authors' Responses:

1. The Fe-Cr clusters varied in size from approximately 5 to 15 nm. Most of the Fe-Cr clusters were spheroidal, and some were more rod-like. The Fe-Ni clusters, which were disc-shaped, had a diameter approximately between 5 and 20 nm. According to TEM examinations, <a>-loop diameters in LK3/L Zircaloy-2 exposed to BWR operation should be about 5 nm.[1] This diameter is in the lower part of the range of our observed cluster sizes, but it is possible that the clusters in APT appear to be slightly larger than the true size.

2 and 3. So far, we can estimate the number density of <a> loops only based on the cluster number density, which is in the approximate range $0.5–1.2 \times 10^{24}$ m^{-3} (identification is challenging due to large variations in cluster size and composition). The <a>-loop number densities of our specific materials have not been measured using other techniques. In previous work the cluster number density determined by APT[2] has been observed to be higher than the <a>-loop number density observed

by TEM.[1] This discrepancy is likely due to the smallest <a> loops not being observed in the TEM analysis.[3] Alternatively, there might be more than one cluster associated with each loop, or there might be clusters that are not directly associated with <a> loops, although they are located in layers typical of <a> loops. Small clusters might be located at vacancy clusters that have not evolved to loops. However, the most straightforward interpretation is that there is one cluster per <a> loop.

1. A. Harte, D. Jädernäs, M. Topping, P. Frankel, C. P. Race, J. Romero, L. Hallstadius, E. C. Darby, and M. Preuss, "The Effect of Matrix Chemistry on Dislocation Evolution in an Irradiated Zr Alloy," *Acta Materialia* 130 (2017): 69–82, https://doi.org/10.1016/j.actamat.2017.03.024
2. J. Eriksson, G. Sundell, P. Tejland, H.-O. Andrén, and M. Thuvander, "Nanoscale Chemistry of Zircaloy-2 Exposed to Three and Nine Annual Cycles of Boiling Water Reactor Operation—An Atom Probe Tomography Study," *Journal of Nuclear Materials* 561 (2022): 153537, https://doi.org/10.1016/j.jnucmat.2022.153537
3. T. Ungár, P. Frankel, G. Ribárik, C. P. Race, and M. Preuss, "Size-Distribution of Irradiation-Induced Dislocation-Loops in Materials Used in the Nuclear Industry," *Journal of Nuclear Materials* 550 (2021): 152945, https://doi.org/10.1016/j.jnucmat.2021.152945.

Question from Aylin Kucuk, EPRI:—Have you measured α-Zr grain boundary segregation of iron, chromium, tin, and nickel in unirradiated Zircaloy-2 materials? If so, have you studied how α-Zr grain boundary segregation varies with different alloy heat treatment?

Authors' Response:—We have (using voltage pulsing) made APT observations of grain boundary segregation of iron and nickel in unirradiated (one grain boundary) and irradiated (two grain boundaries) Alloy 2, in which chromium was not present at the grain boundaries. Furthermore, in previous work (using laser pulsing) on irradiated LK3/L Zircaloy-2, we have also observed Sn and very small amounts (lower than the concentrations of iron and nickel) of chromium at grain boundaries.[2] Grain boundaries in the irradiated materials were from close to the metal/oxide interface, which means they probably were subgrain boundaries created during plastic deformation caused by the stresses exerted by the growing oxide. We have not studied how grain boundary segregation in unirradiated material varies with heat treatment.

Question from Philipp Frankel, University of Manchester:—The α-annealed plate did not show different corrosion performance in the quenched or annealed condition. Is it known whether the difference in matrix concentration/composition remains during corrosion testing, or is the autoclave temperature sufficient to redistribute the iron/chromium?

Authors' Response:—Autoclave testing was performed in steam at two different temperatures, 415 and 500°C.[4] Diffusivities are sufficient to reach equilibrium

during autoclaving (certainly for iron and nickel and probably for chromium),[5] so there should be some redistribution of iron and chromium, but the solubilities are probably very low. We did not perform measurements of the matrix content of autoclaved specimens. Even if we would have measured the content after autoclave exposure, it would probably not give the content during testing because the cooling from the test temperature to room temperature was slow, so we should get values similar to furnace-cooled samples. However, as there was essentially no difference in corrosion between the differently heat-treated materials, we can still conclude that the initial matrix content of iron and chromium does not affect the corrosion properties.

4. B. Hutchinson, B. Lehtinen, M. Limbäck, and M. Dahlbäck, "A Study of the Structure and Chemistry in Zircaloy-2 and the Resulting Oxide after High Temperature Corrosion," in *Zirconium in the Nuclear Industry: 15th International Symposium*, ed. B. Kammenzind and M. Limbäck (West Conshohocken, PA: ASTM International, 2009), 269–284, https://doi.org/10.1520/STP48141S
5. G. M. Hood, "Point Defect Diffusion in α-Zr," *Journal of Nuclear Materials* 159 (1988): 149–175, https://doi.org/10.1016/0022-3115(88)90091-8

Questions from Patrick Burr, UNSW Sydney:

1. Alloy 2 has a lower hydrogen pickup than LK3, and the main difference between them is the iron and chromium content, right?
2. Here you show us that there is no difference in iron and chromium content in the matrix after irradiation. If anything, there is less iron and chromium in solid solution in Alloy 2 (but probably within error), so how does the added iron and chromium reduce hydrogen pickup?

Authors' Responses:

1. Yes, Alloy 2 has lower hydrogen pickup than LK3/L Zircaloy-2, and the main difference between them is the higher iron and chromium content of Alloy 2.
2. We are surprised that there is no significant difference in the matrix content between the two alloys after reactor operation (here the matrix content includes the irradiation-induced clusters). One possible explanation for the difference in hydrogen pickup might be differences in the size, number density, and composition of SPPs. If the matrix content of iron and chromium after irradiation is essentially the same in both alloys, there should be more of these elements in SPPs in Alloy 2. No detailed SPP analysis comparing the same lots of both alloys before and after reactor operation has been performed. Such an analysis, although practically difficult to perform, could give information on this matter. However, it is known from previous work that there are large local variations within irradiated Zircaloy-2,[2,6] so it cannot be completely excluded that this type of variations has influenced our

observations. It is possible (if not likely) that the estimations are skewed due to the very small volumes probed. We have measured a tip containing a partly dissolved $Zr(Fe,Cr)_2$ SPP (42 at.% chromium and 2 at.% iron), and after approximately 100 nm from it there is virtually no chromium (0.09 at.%) and little iron (0.28 at.%). This illustrates that the position of the lift-out has a large influence.

6. G. Sundell, M. Thuvander, P. Tejland, M. Dahlbäck, L. Hallstadius, and H.-O. Andrén, "Redistribution of Alloying Elements in Zircaloy-2 after In-Reactor Exposure," *Journal of Nuclear Materials* 454 (2014): 178–185, https://doi.org/10.1016/j.jnucmat.2014.07.072

Question from Bruce Kammenzind, Naval Nuclear Laboratory, Bettis Laboratory:—I believe you state a conclusion that iron levels in the matrix of zirconium alloys do not influence corrosion based on autoclave corrosion studies that showed water-quenched Zircaloy-type materials in your study to corrode similarly to very slowly cooled materials. I believe, however, that in a symposium paper from several years ago discussing the in-reactor corrosion behavior of the LK series of Zircaloy-2 alloys, LK Zy-2 with less aging after the final β quench (e.g., LK2) corroded worse in reactor than LK3 with more post-β-quench aging. Might the autoclave observation that you make here be more an indication that the mechanism by which iron in the matrix promotes increased corrosion requires active in-reactor irradiation conditions?

Authors' Response:—We conclude that the influence of initial matrix content of iron (and chromium) on autoclave corrosion is negligible in comparison with the influence of the total iron and chromium content (which affects the volume fraction of SPPs). The improved in-reactor corrosion of LK3 Zircaloy-2 over that of LK2 has been attributed to the larger SPPs and possibly also to the slightly higher iron content of LK3. As we observe in our as-produced LK3 material, there is almost no iron, chromium, or nickel in the matrix, whereas there are several hundred wt. ppm after reactor exposure. There is thus obviously a much higher alloying element content in the matrix (including clusters) after reactor operation than after autoclave testing. Any effect on corrosion by iron (or chromium or nickel) in the matrix should thus most likely be more important in reactor.

Question from Michael Preuss, Monash University and University of Manchester:—Do you see any difference in the way iron segregates to what you assume to be <a> loops? I am asking because I would expect significant differences between how iron segregates to interstitial versus vacancy loops.

Authors' Response:—We see a difference between Fe-Cr clusters and Fe-Ni clusters; the former appear spheroidal or rod-like, whereas the latter appear disc-shaped. Both types of clusters are located in layers that are typical of layers of

<a> loops. We cannot, however, directly see the loops using APT to determine how the clusters are related to the loops and whether there is a difference in segregation between vacancy and interstitial loops. Hence, it is possible that there is clustering at only one type of <a> loop, or that Fe-Cr and Fe-Ni clusters are related to different types of <a> loops. It might be possible to determine any correlation between loop character and segregation of alloying elements by correlative TEM and APT.